ISSN 1069-3513, Izvestiya, Physics of the Solid Earth, 2007, Vol. 43, No. 1, pp. 75–90. © Pleiades Publishing, Ltd., 2007.

Why the Sacramento Delta Area Differs from Other Parts of the Great Valley: Numerical Modeling of Thermal Structure and Thermal Subsidence of Forearc Basins[1]

V. O. Mikhailov[a], T. Parsons[b], R. W. Simpson[b], E. P. Timoshkina[a], and C. Williams[b]

[a] *Schmidt Institute of Physics of the Earth, Russian Academy of Sciences, Bol'shaya Gruzinskaya ul. 10, Moscow, 123995 Russia*

[b] *US Geological Survey, Menlo Park, CA USA*

Received June 8, 2006

Abstract—Data on present-day heat flow, subsidence history, and paleotemperature for the Sacramento Delta region, California, have been employed to constrain a numerical model of tectonic subsidence and thermal evolution of forearc basins. The model assumes an oceanic basement with an initial thermal profile dependent on its age subjected to refrigeration caused by a subducting slab. Subsidence in the Sacramento Delta region appears to be close to that expected for a forearc basin underlain by normal oceanic lithosphere of age 150 Ma, demonstrating that effects from both the initial thermal profile and the subduction process are necessary and sufficient. Subsidence at the eastern and northern borders of the Sacramento Valley is considerably less, approximating subsidence expected from the dynamics of the subduction zone alone. These results, together with other geophysical data, show that Sacramento Delta lithosphere, being thinner and having undergone deeper subsidence, must differ from lithosphere of the transitional type under other parts of the Sacramento Valley. Thermal modeling allows evaluation of the rheological properties of the lithosphere. Strength diagrams based on our thermal model show that, even under relatively slow deformation (10^{-17} s^{-1}), the upper part of the delta crystalline crust (down to 20–22 km) can fail in brittle fashion, which is in agreement with deeper earthquake occurrence. Hypocentral depths of earthquakes under the Sacramento Delta region extend to nearly 20 km, whereas, in the Coast Ranges to the west, depths are typically less than 12–15 km. The greater width of the seismogenic zone in this area raises the possibility that, for fault segments of comparable length, earthquakes of somewhat greater magnitude might occur than in the Coast Ranges to the west.

PACS numbers: 91.45.Hc

DOI: 10.1134/S1069351307010089

1. INTRODUCTION

While many excellent studies have been devoted to thermal modeling of subduction zones (e.g., [McKenzie, 1969, 1970; Hsui and Toksöz, 1979; van der Beukel and Wortel, 1988; Honda, 1985; Dumitru, 1991; Spencer, 1994; Davis, 1999; Devaux et al., 2000]), we are unaware of any attempt to make quantitative comparisons of forearc basin subsidence with numerically predicted values. A possible explanation is that modeling of forearc basin subsidence calls for the solution of a number of different problems. First, the thermal structure of forearc lithosphere is strongly influenced by the subduction process and depends on the rate and angle of subduction and the age of the approaching slab [Dumitru, 1991; Bohannon and Parsons, 1995]. In the subduction zone to the west of the Great Valley, California, these parameters have changed considerably during the last 150 Myr [Engebretson et al., 1985]. Second, forearc basins develop on top of an oceanic lithosphere, which continues subsiding in the course of its cooling. Thus, an initial temperature should be assigned based on the nonsteady-state temperature profile of an oceanic lithosphere of corresponding age. Third, thermal subsidence usually forms the long-term background for a number of short-term events, such as regional compression, arrival of terrains, etc. Thus, subsidence curves of forearc basins contain at least three components: (1) subsidence or uplift as a result of the dynamics of the subduction zone, including temporal variations in subduction parameters; (2) thermal subsidence of oceanic lithosphere, as the temperature distribution is in a nonsteady state at the beginning of subduction; and (3) local tectonic events. Close to trenches, subduction erosion (see, e.g., [Scholl et al., 1980]) and variation in coupling along plate interfaces could also be important.

In this paper, we consider a geodynamic model of thermal evolution and tectonic subsidence of a forearc basin and calibrate it using data from three oil and gas exploratory wells in the Sacramento Valley and one measured section across the Diablo Range to the southeast of the valley. Model predictions compare favorably

[1] The text was submitted by the authors in English.

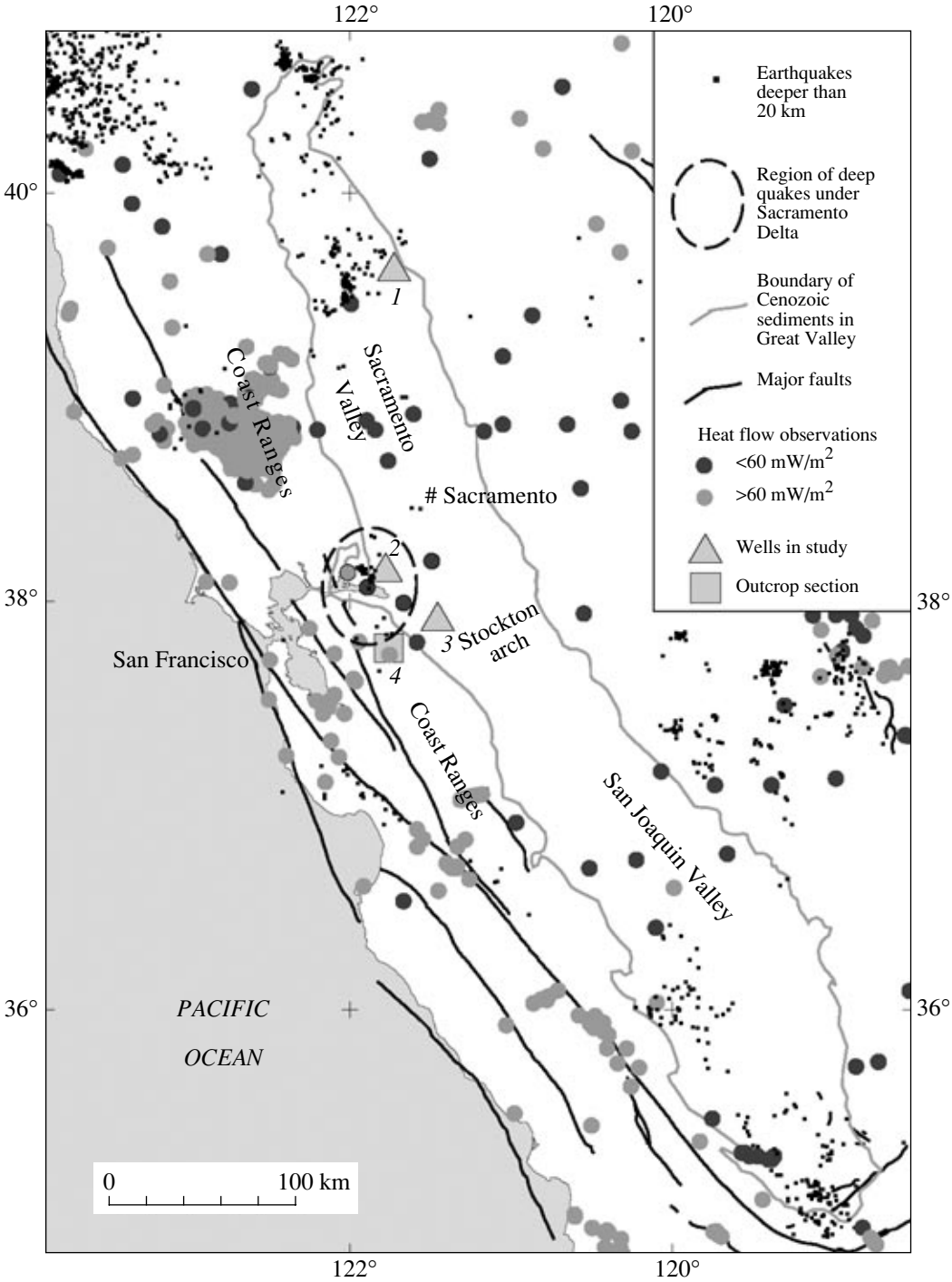

Fig. 1. Map of the Great Valley of California and surrounding areas. Small black dots are earthquakes, relocated using the double-difference method [Ellsworth et al., 2000], with depths greater than 20 km. The deep cluster of earthquakes under the Sacramento Delta is surrounded by the dashed line. Deep earthquakes in the northern part of the Sacramento Valley are related to the subducting Juan de Fuca Plate (e.g., [Benz et al., 1992]). The locations of the three logged wells (*1, 2, 3*) and the Mt. Diablo sedimentary section (*4*) used to define subsidence curves are also indicated. Heat flow values are indicated by circles filled with black or gray. Heat flow values in the delta region are new preliminary values.

with available data on the thermal and subsidence history of the Sacramento Valley as well as paleotemperature observations. Last, we use the temperature profile predicted by the model to estimate the present-day strength of the lithosphere under the Sacramento Delta region in order to better understand the origin of deep earthquakes in this region. Indeed, an anomalous cluster of earthquakes under the Sacramento Delta region

extends to a depth of ~20 km (Fig. 1), whereas hypocentral depths in the Coast Ranges to the west are typically shallower than 12–15 km [Wong et al., 1988; Oppenheimer and Macgregor-Scott, 1992]. The unusually deep (~20 km) seismicity in this region may be a manifestation of higher strength of the lower crust in comparison to other parts of the Sacramento Valley. This can result from a different thermal state and/or from a different composition of crustal rocks.

First, we briefly review the data on the structure and evolution of the Great Valley, in particular, for its northern part, the Sacramento basin, and present tectonic subsidence curves at the locations of four sedimentary sections. Next, we combine two thermal models: one quantifying the thermal subsidence of a forearc basin, taking into account changes in subduction rate and age of the approaching plate, and the other quantifying the thermal subsidence of cooling oceanic lithosphere, taking into account the blanketing effect of sediments and the crystallization of basalt melt. Last, we compare our thermal model to available geothermal data for the Sacramento Delta region, including present-day heat flow and estimates of paleotemperature, and calculate strength diagrams based on the inferred temperature distribution in order to explain the anomalous deep cluster of earthquakes in this area.

2. ORIGIN, STRUCTURE, AND EVOLUTION OF THE GREAT VALLEY

2.1. Data on the Origin and Evolution of the Great Valley

The structure of California's Great Valley has been studied by various methods, including seismic refraction and reflection studies, numerous logged boreholes, and gravity and magnetic surveys. Many events in its development, revealed in the variation in thickness and facies composition of sedimentary layers, timing of volcanism, and phases of folding and faulting, correlate with changes in the rate and direction of subduction to the west (e.g., [Dickinson and Snyder, 1979; Page and Engebretson, 1984; Moxon and Graham, 1987]).

The Great Valley of California is a Mesozoic–Cenozoic forearc basin formed to the west of the Sierra Nevada volcanic arc. Sedimentary fill of the valley forms an elongate prism that thickens rapidly to the west, where the basement depth probably exceeds 14 km [Wentworth et al., 1995]. On the west side, a thick Upper Jurassic to Upper Cretaceous (Campanian to Maastrichtian) turbidite sequence is exposed in the eastern Coast Ranges deposited upon Upper Jurassic (153–165 Ma) ophiolites [Hopson et al., 1981]. In the eastern part of the valley, numerous oil and gas exploratory wells have never found strata older than Late Cretaceous. Seismic data fail to provide strong constraints on the eastern limit of the Upper Jurassic–Lower Cretaceous layers; probably this limit coincides with a pronounced magnetic anomaly stretching along the central part of the Great Valley [Beyer, 1988]. The E–W-trending Stockton arch separates the valley into two basins: the Sacramento basin to the north and the San Joaquin basin to the south (Fig. 1).

A forearc basin became established in the region by the Late Jurassic (e.g., [Hey et al., 1988]). Dickinson et al. [1987] suggested that the Nevadan orogeny and establishment of the Great Valley as a forearc sedimentary basin was the result of a mid-Jurassic collision with a migratory oceanic arc. From the Tithonian through the Maastrichtian, the Great Valley was a deep-marine basin, bounded on the west by the subduction zone now represented by rocks of the Franciscan complex. Paleocurrent indicators in outcrops of Upper Jurassic and Lower Cretaceous turbidites on the west side of the valley show evidence of flow to the south parallel to the continental margin, suggesting that by this time the Franciscan accretionary wedge had achieved sufficient bathymetric relief to maintain the Great Valley as a starved deep-marine basin [Ingersol, 1979].

Near the end of the Cretaceous, the character of the deposystems changed significantly. In the Maastrichtian, the Sacramento basin fan facies were replaced by periodically prograding deltaic deposits [Graham, 1987]. This shoaling may simply reflect infilling of the bathymetric relief, or, alternatively, it could be the result of a proposed Late Cretaceous and Early Tertiary decrease in the angle of subduction [Dickinson et al., 1987]. It is worth noting that a change in the subduction angle inferred from a shift of volcanism is one of several explanations [Bohannon and Parsons, 1995]. Emplacement of the granitic terrain of the Salinian block along the proto-San Andreas fault occurred in the Late Paleocene, at approximately 55 Ma [Graham, 1987]. This event forced a major reorganization of the Great Valley basin, in particular, its separation into the Sacramento and San Joaquin subbasins by the transverse Stockton arch. Another explanation of the Late Cretaceous–Early Tertiary events is oblique subduction with a northerly to northeasterly convergence direction [Engebretson et al., 1985]. During the Paleogene, the Sacramento basin was a shelved forearc basin subjected to episodic transgressions and regressions. At the end of the Paleogene, a depositional hiatus related to widespread regression extended through the Great Valley basins. Neogene to Recent sedimentation in the Sacramento Valley was entirely nonmarine except in parts of the San Francisco Bay area [Beyer, 1988].

Many tectonic events in the period of the last 30 Myr correlate well with the interaction between the East Pacific Rise spreading center and North America. This interaction resulted in the propagation of the San Andreas transform fault system and the northwestward migration of the Mendocino triple junction. (For detailed consideration of this period, see [Beyer and Bartow, 1987; Beyer, 1988; Bohannon and Parsons, 1995].) The very complicated history of the last 30 Myr is not under discussion here because, in a first-order

consideration of the thermal structure of the Great Valley, one can neglect effects that took place relatively far to the west in the region of the San Andreas fault (this is especially true for the Sacramento basin, where these events occurred considerably later). Results of Furlong [1984] support this assumption: when modeling the thermal effect of the northward-migrating Mendocino triple junction, he did not find an increase in calculated heat flow in the Great Valley area.

2.2. Crustal Structure and Seismicity

The crustal structure of the southern part of the Sacramento basin and Sacramento Delta depocenter has been studied by a seismic refraction profile [Eaton, 1963] running from San Francisco through the Sacramento Delta to the Sierra Nevada and by the BASIX seismic survey (e.g., [Hole et al., 2000]). Eaton [1963] estimated the Moho depth in the Sacramento basin to be as shallow as 20 km. Prodehl [1979] reanalyzed this profile and estimated the Moho depth as 22–23 km. BASIX data overlap only the western edge of the Sacramento Delta region, suggesting the same range for the crustal thickness, and more than 12 km of low-velocity sediments in the western part of the Sacramento Delta. Even though the crustal structure of the deepest parts of the Sacramento basin remains unclear, it is obvious that it differs considerably from the other parts of the Great Valley. Indeed, the thickness of the sediments in the Sacramento Delta area exceeds 14 km [Wentworth et al., 1995] or even 16–18 km [Beyer, 1988], whereas the depth to the Moho is estimated as 22–23 km. Thus, the crystalline crust in this area ranges in thickness from 5 to 10 km, which is similar to the average thickness of most oceanic crust. Several seismic profiles, characterizing mainly the San Joaquin basin and the northern part of the Sacramento basin, yield a thickness of the crystalline crust of 21–26 km (e.g., [Holbrook and Mooney, 1987; Wentworth et al., 1987; Mooney and Weaver, 1989]). This thickness could correspond either to oceanic crust stacked on top of Sierran volcanic-arc crust [Wentworth et al., 1987; Godfrey et al., 1997], to thickened sheared/intruded crust [Page and Brocher, 1993; Holbrook et al., 1996], or to Great Valley ophiolite crust [Jachens et al., 1995].

The Sacramento Valley appears to have undergone a moderate level of crustal deformation, at least in the Quaternary [Wong, 1987]. Figure 1 shows the distribution of double-difference relocated earthquakes deeper than 20 km in a part of Northern California [Ellsworth et al., 2000] and outlines the region of deeper events in the Sacramento Delta area. Historic earthquakes with magnitudes of 6–6.5 have occurred along the western margin of the Great Valley to the north and south of this cluster, and an $M \leq 6.0$ event in 1889 may have occurred within the cluster [Bakun, 1999]. Earthquakes in the cluster have been attributed to activity on the near-vertical Pittsburg/Kirby Hills and Kirker faults [McCarthy et al., 1994], although complex nonvertical structures, including blind thrusts, tectonic wedges, and mid-crustal decollements, have been identified along the eastern margin of the Sacramento Valley (e.g., [Weber-Band et al., 1997; Unruh and Lettis, 1998; O'Connell et al., 2001]), some of which may separate near-surface structures from the deep seismogenic faults within the basement. Hypocenters from the Northern California Seismic Net relocated using double-difference techniques [Ellsworth et al., 2000] do not define any single, clear, through-going structure in this cluster, although several local planes of limited extent, both vertical and dipping, are defined by alignments of hypocenters. Simultaneous inversion of earthquake and seismic refraction traveltimes yielded depths for earthquakes in the cluster that were shallower than double-difference depths (mostly less than 20 km, compared with 23 km) [Hole et al., 2000, Plates 1, 2], although the cluster still stands out by virtue of its greater depth extent.

2.3. Heat Flow and Paleotemperature

Heat flow in the Great Valley is lower in the western part than in the central and eastern parts, but everywhere is lower than in the Coastal Ranges [Sass et al., 1971]. Published heat flow measurements [Sass et al., 1971, 1982, 1997; Lachenbruch and Sass, 1980; Wang and Monroe, 1982; Williams et al., 1994] are shown in Fig. 1, along with preliminary values from new measurements in the Sacramento Delta region. The important feature of heat flow in the region is a rapid decrease in values from the Coast Ranges to the Great Valley. Heat flow in the Great Valley is typically less than 45 mW/m^2 and averages 30–35 mW/m^2.

Using corrected well log temperatures from more than 3000 wells, Lico and Kharaka [1983] concluded that the temperature gradient in Sacramento basin sedimentary rocks ranges from 18 to 25°C/km. Based on different geochemical data, Zieglar and Spotts [1978] estimated thermal gradients in the Great Valley sediments for the period from the Cretaceous to the present to be in the range 22–35°C/km. Dumitru [1989] arrived at considerably lower thermal gradients (9°C/km in the Tertiary and 15°C/km in the Cretaceous) using results of fission track analysis. He may have overestimated burial depth by (1) assuming that the thickness of the Upper Jurassic–Lower Cretaceous layers in the eastern part of the Coast Ranges was not increased tectonically by later deformations (cf. [Wentworth and Zoback, 1989]) and (2) increasing burial depth by adding the Upper Cretaceous–Lower Paleocene deposits, which are now present only in the eastern part of the Great Valley.

3. SUBSIDENCE HISTORY

Different types of lithosphere should possess different thermal structures and, as a consequence, should exhibit different long-term subsidence histories. Thus,

different thermal models of the deep basin structures can be tested against available lithologic and seismic data on the structure and subsidence history of the Great Valley sedimentary basin. To investigate the subsidence history of the Great Valley, we compiled borehole data collected by Moxon [1990] with data from a USGS borehole database [Brabb et al., 2001]. We used eustatic sea level curves of Haq et al. [1987], correcting for both long-term and short-term sea level changes and porosity–depth dependences suggested by Stam et al. [1987]. Williams [1997] tested the sensitivity of Great Valley subsidence curves to errors in the input data and demonstrated a low sensitivity to all input parameters except paleobathymetry estimates. Our resulting subsidence curves differ in certain details from those of Moxon [1990], although the main features are the same.

Below, we consider four water-unloaded (i.e., without the load of water filling depressions up to sea level) tectonic subsidence curves corresponding to three wells and one outcrop site situated in different parts of the Sacramento basin (Fig. 2; for locations, see Fig. 1). Curve *1* is from Standard's Dodge Land #1 well; curve *2*, from Chevron's Peter Cook #13 well; curve *3*, from Arco's Mantelly #1 well; and curve *4*; from a Mt. Diablo outcrop section. Details can be found in [Moxon, 1990; Brabb et al., 2001].

Subsidence curve *1* characterizes the northern edge of the basin, curves *2* and *4* describe the subsidence of the Sacramento Delta region, and curve *3* characterizes the southeastern edge close to the Stockton arch. The shaded periods in Fig. 2 correspond to the onset (75–80 Ma) and cessation (40–45 Ma) of the Laramide orogeny [Moxon and Graham, 1987].

We restricted our analysis to the interval from the Late Cretaceous through the Neogene, thus ignoring earlier periods represented by turbidites, because the depth of turbidite formation is poorly constrained. For example, Dickinson et al. [1987] estimate its upper and lower limits as 1500 and 3000 m. This interval is too broad to constrain any subsidence scenario (uncertainty limits are given in Fig. 2 by dashed lines). In addition, it is unclear whether the thicknesses of Upper Jurassic–Lower Cretaceous strata measured across the Diablo Range outcrops represent the real vertical depositional thickness or a composite section resulting from en echelon stacking of deposits of different ages and possibly from different depths (e.g., [Moxon, 1990]). Many sections measured across the outcrops indicate a total composite stratigraphic thickness of Lower Jurassic–Upper Cretaceous strata in excess of 10–15 km, whereas nearby boreholes penetrating to the basement traverse less than 4–6 km of sedimentary rocks [Williams, 1997]. As a result, uncertainty limits for the period before 65–70 Ma (see, e.g., Fig. 2, curves *3*, *4*) are wide enough to accommodate either a horizontal line, corresponding to passive sedimentary infilling of an initial topography [Graham, 1987; Williams, 1997], or a descending curve, corresponding to tectonic control of subsidence [Moxon and Graham, 1987].

Let us consider the main features of Great Valley subsidence revealed by the subsidence curves. It is worth noting that the subsidence curves show the average subsidence over the deposition interval of each stratigraphic section. Because stratigraphic subdivisions in the wells are different (Fig. 2, cf. curves *1*, *3* with curves *2*, *4*), some events registered by one curve can be smoothed and not seen on the others. Subsidence curves *2* and *4* for the Sacramento depocenter area are similar for the last 80 Myr. They display a number of short-term tectonic events taking place on the background of a total long-term subsidence that started before 80 Ma. In particular, the uplift in curve *4* between 80 and 60 Ma can be attributed to an uplift of the western edge of the Sacramento basin that started in the Late Cretaceous [Zieglar and Spotts, 1978; Dickinson et al., 1987]. This uplift was followed by several relatively fast subsidence events that occurred during the Laramide orogeny. One of these events occurred about 55 Ma and coincides with the arrival of the Salinian block followed by a relatively deep and long subsidence period between 50 and 42 Ma.

We are particularly interested in the long-term component of tectonic subsidence, which is likely linked to the temporal and spatial thermal changes within the lithosphere and underlying mantle. To estimate the influence of the various factors that might determine the long-term subsidence of forearc lithosphere, we constructed a numerical thermal model, which is described in the next section.

4. THERMAL MODEL OF FOREARC LITHOSPHERE

4.1. Statement of the Problem

The temperature and subsidence of forearc basins are controlled by changes in rate and age (thickness, temperature profile) of the subducting plate; by nonsteady-state temperature in the overriding plate at the beginning of subduction; and by the blanketing effect of sediments, which can exceed 15 km in forearc basins. In our modeling, we used thermal conductive/advective equations with a preassigned velocity field. The heat transfer equation is linear, so, by choosing the boundary conditions properly, the problem can be subdivided into two parts: thermal subsidence of the forearc lithosphere refrigerated by the subducting plate (taking into account changes over time in the rate and age of the approaching plate) and thermal age-dependent subsidence of the upper plate. Let us now consider both thermal problems.

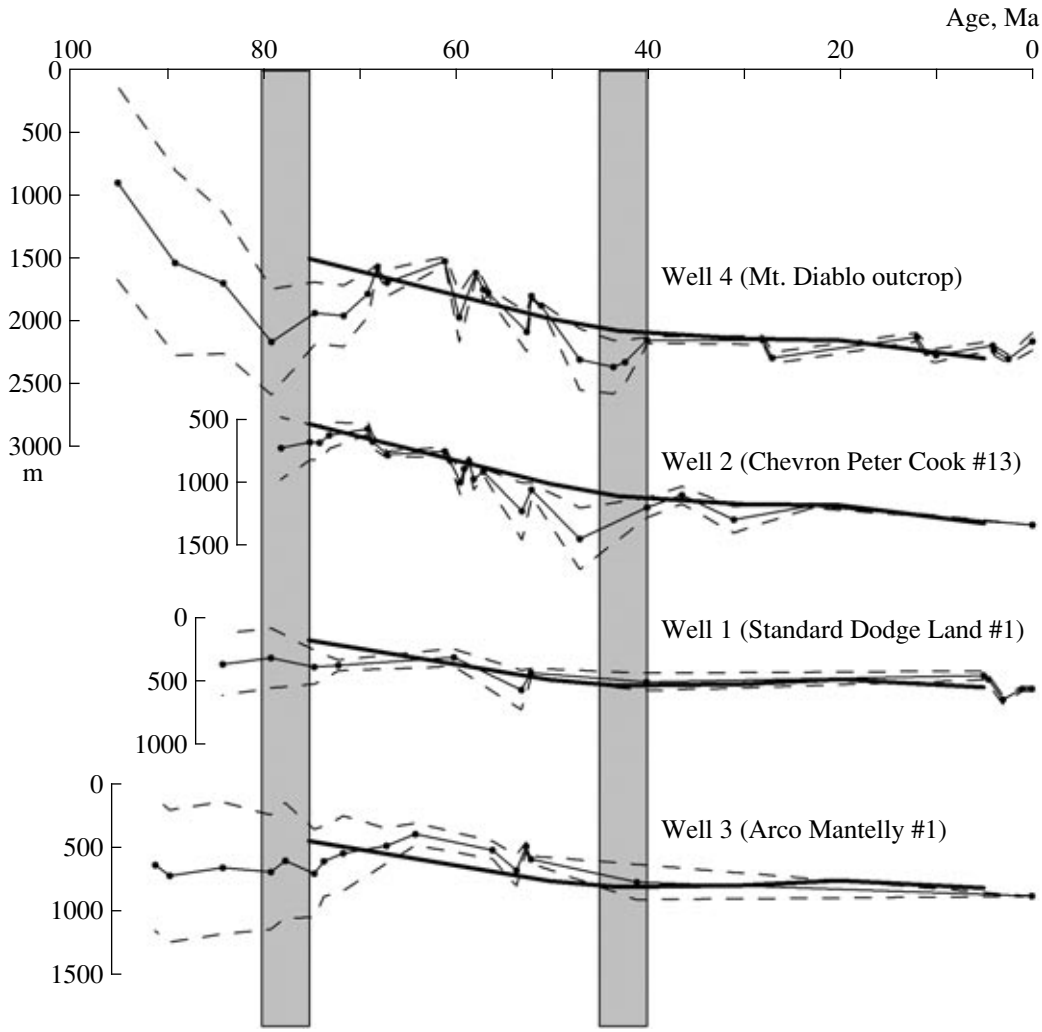

Fig. 2. Tectonic water-unloaded subsidence curves for three wells (1, 2, 3) and one measured outcrop section (4) situated in different parts of the Sacramento Valley. For location of wells and section, see Fig. 1. Dashed lines show upper and lower limits corresponding to different sedimentation depth estimates. The solid black line with circles corresponds to the average value of sedimentation depth. The thick black line for well 2 and outcrop 4 shows subsidence of a forearc basin, situated on 150-Ma oceanic lithosphere, caused by changes in subduction rate and age of the approaching plate [Engebretson et al., 1985; Stock and Molnar, 1988]. The thick black lines for wells 1 and 3 show subsidence of a forearc basin situated on transitional lithosphere. The shaded periods at the subsidence curves mark the onset (75–80 Ma) and cessation (40–45 Ma) of Laramide orogeny in this region [Moxon and Graham, 1987].

4.2. Thermal Model of a Subduction Zone

There are several types of thermal models of oceanic subduction zones, including 1-D analytical models [McKenzie, 1969, 1970; Davis, 1999], 2-D thermal models with preassigned kinematics [van der Beukel and Wortel, 1988; Dumitru, 1991; Spencer, 1994; Bohannon and Parsons, 1995], and formal thermomechanical models solving appropriate equations of motion and heat transfer [Hsui and Toksöz, 1979; Honda, 1985; Devaux et al., 2000]. To estimate the heat balance basin subsidence in the forearc environment, we used results of Bohannon and Parsons [1995]. Their model considers conductive and advective heat transport within a volume that includes both the subducting oceanic and the overriding plates as well as the part of the upper mantle containing the sinking slab. The rate of convergence and the age of the subducting plate were assigned by averaging data of Engebretson et al. [1985] and Stock and Molnar [1988]. Subduction was allowed to progress over the period from 90 to 5 Ma at an angle of 15°, the same as the present-day dip of the Gorda and Juan de Fuca slabs [Parsons et al., 1998]. A constant dip of the slab was retained through the modeling period even though the east-to-west rollback of volcanism that occurred between about 42 and 15 Ma has been attributed by some authors to subduction steepening; e.g., Coney and Reynolds [1977], Engebretson et al. [1985], and Stock and Molnar [1988] suggested a slowing in the convergence rate at about 43 Ma. This might have initiated a westward recession of isotherms marking the coherent edge of the slab in the thermal model (Fig. 3).

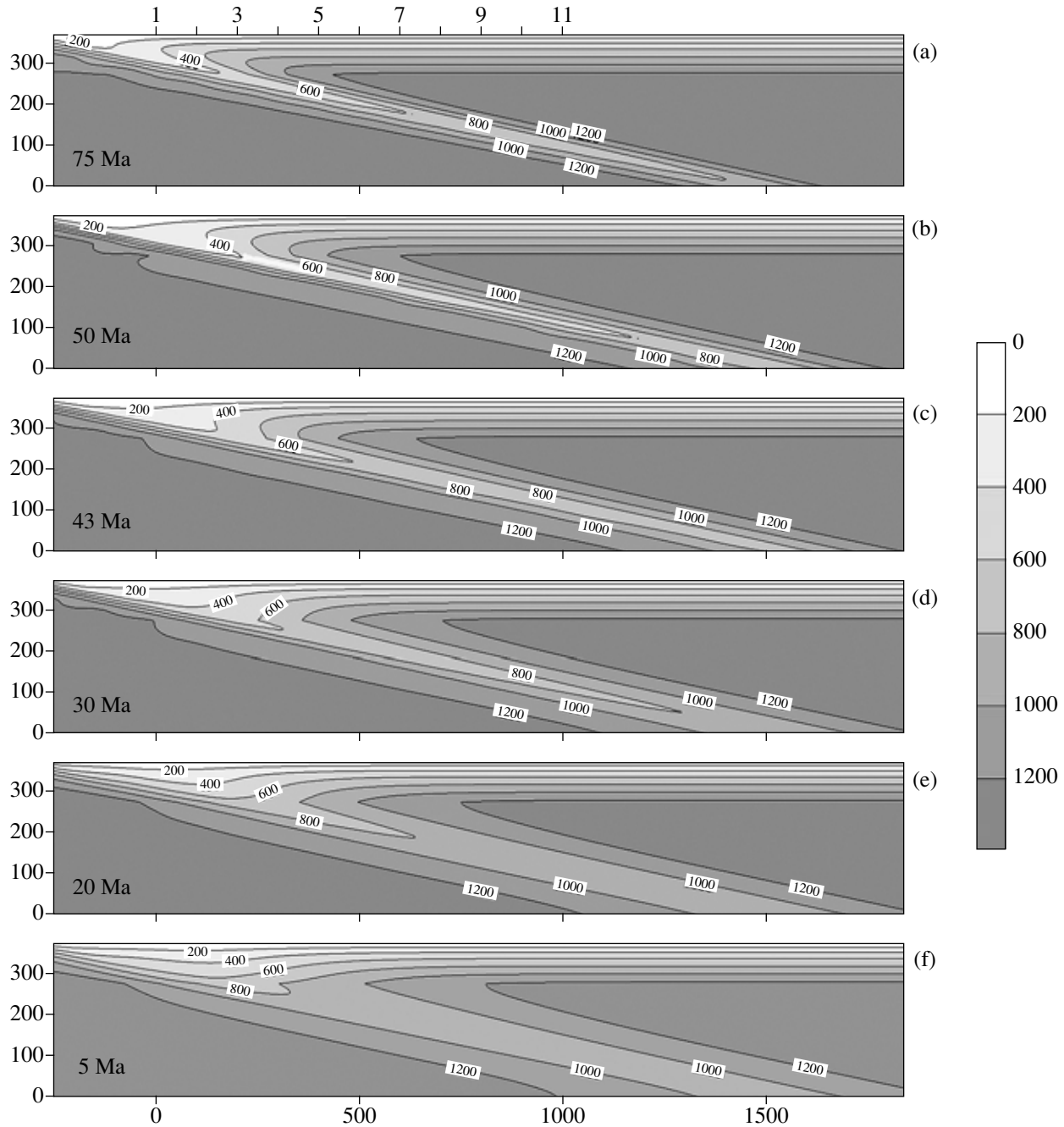

Fig. 3. Thermal structure of Farallon subduction zone for six moments in time [Bohannon and Parsons, 1995].

It permitted Severinghaus and Atwater [1990] and Bohannon and Parsons [1995] to conclude that the slab never got any steeper and that the locus of volcanism simply occurred above the eastern edge of coherence in the slab. Following the suggestions of Underwood [1989] and Dumitru [1991], shear stresses in the subduction zone were assumed to be as small as 10–30 MPa; this allows one to neglect the effect of corner flow [Peacock, 1996].

Distributions of temperature within the lithosphere and mantle for six moments in time are shown in Fig. 3. This figure demonstrates that isotherms receded up to the west due to the reduction in rate and the decrease in age of the lithosphere entering the trench from 50 to 30 Ma (Figs. 3b–3d). Before this time interval, isotherms moved down the slab, apparently because of the higher subduction rate. From 30 to 5 Ma (Figs. 3d–3f), the isotherms in the slab south of the Mendocino triple junction continued to recede back toward the trench after Pacific/North American plate contact, causing the coherent leading edge of the slab to lie only about 400 km east of the trench by 20 Ma (Fig. 3e). To inves-

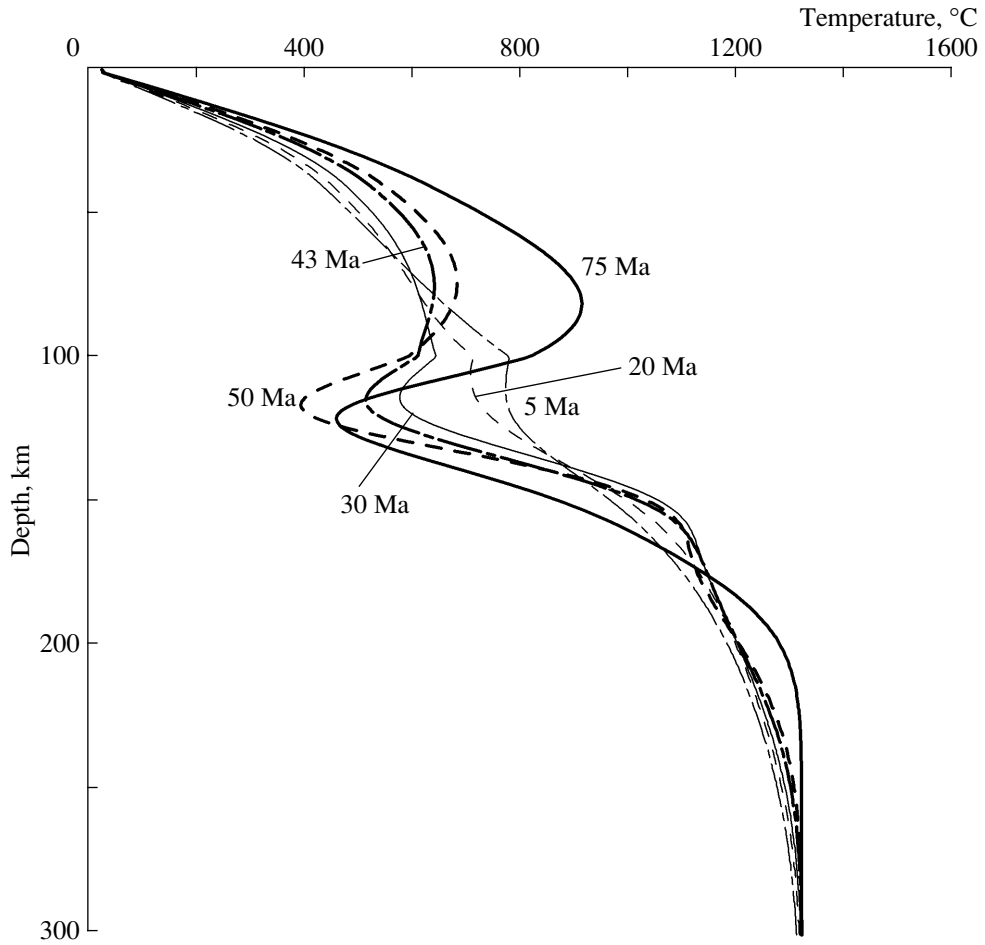

Fig. 4. Distribution of temperature with depth in a forearc basin at 100 km distance from the trench (location *2* in Fig. 3a) for the same six moments in time as in Fig. 3 (numbers show ages).

tigate temperature changes in the upper 400 km below the forearc, we present temperature versus depth plots (Fig. 4) for a vertical cross section situated at 100 km from the trench (Fig. 3a, point *2*). Figure 4 shows considerably lower temperatures at the depth of the sinking slab (below 80 km). Rapid changes in temperature between 75 and 50 Ma were caused by an increase in subduction rate. After 50 Ma, the temperature within the slab below the forearc basin increased, while at the same time it decreased in the mantle above and below the slab, forming a smoother distribution.

Let us now consider subsidence of the forearc basin. Calculated subsidence curves for locations *1–11* are presented in Fig. 5 (locations are indicated at the top of Fig. 3). These curves were obtained by integrating temperature over depth for different moments in time, using a thermal expansion coefficient of 3×10^{-5} 1/°C. Zero (reference) elevation was assigned to the subsidence depth at 75 Ma. Calculated subsidence curves in Fig. 5 show rapid subsidence between 75 and 50 Ma for all of the points situated within the forearc as a result of the rapid increase in subduction rate. Slower vertical movements after 50 Ma result from a decrease in the age of the subducting slab, a decrease in subduction rate, and a reequilibration (smoothing) of the sharp temperature gradient that had formed between 75 and 50 Ma. The total subsidence since 50 Ma appears to be small: it is close to zero at locations *2* and *3* and increases to the east to 100–200 m at locations *4–11*. Flattening of the subsidence curves after 45 Ma is consistent with establishment of shallow marine or continental sedimentation in the Sacramento Delta during the Late Paleogene–Neogene (e.g., [Beyer, 1988]). Short-term fluctuations in the subsidence curves between 50 and 43 Ma were apparently caused by modeled establishment of thermal equilibrium after the rapid acceleration of subduction between 75 and 50 Ma.

We estimate the distance from the Sacramento Delta region to the trench to have been 200 km, corresponding to location *3* (Fig. 3) to characterize subsidence caused by subduction. Let us now consider subsidence caused by cooling of an oceanic lithosphere under the delta sediments.

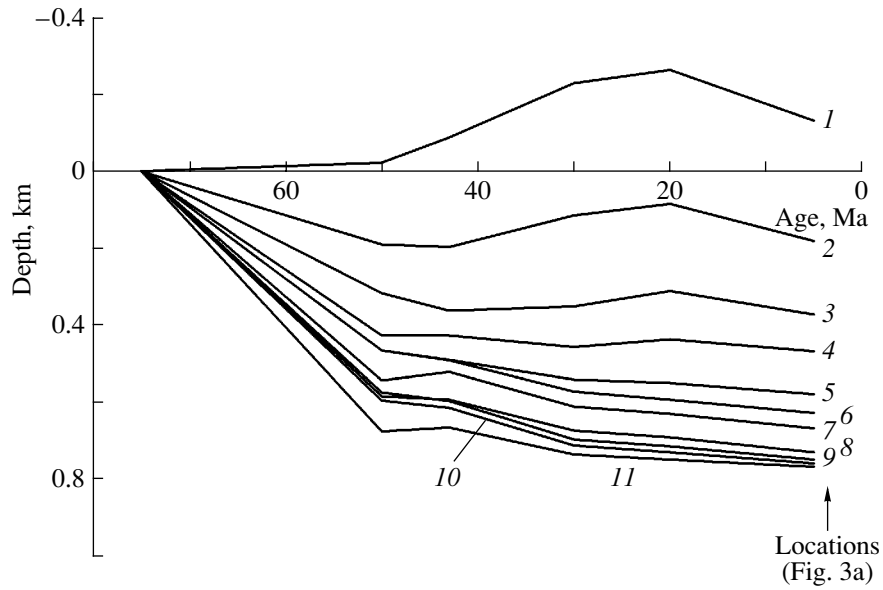

Fig. 5. Water-unloaded subsidence curves for 11 locations situated at different distances from the trench. Locations are indicated in Fig. 3a. Note that changes in the rate of subduction and in the age of the sinking slab produce different vertical movements close to the trench (locations *1–3*) and in the forearc basin (locations *4–11*).

4.3. Thermal Model of Cooling Oceanic Lithosphere

Numerical modeling of the systematic decrease in heat flow and increase in depth of oceanic lithosphere with age has been attempted by many researchers (for a detailed bibliography, see Stein and Stein [1992]). There are three basic models of the thermal subsidence of aging oceanic lithosphere: (1) a cooling plate of a constant thickness [Langseth et al., 1966; McKenzie, 1967], (2) a plate that thickens as it cools due to crystallization of basalt melt at the lithosphere–asthenosphere boundary [Parker and Oldenburg, 1973], and (3) a cooling half-space [Davis and Lister, 1974]. All these models approximate the $\sqrt{t}$ dependence of the oceanic depth and the $1/\sqrt{t}$ dependence of the heat flow for ages less than 75 Ma fairly well, where t is the age of the lithosphere. For greater ages, the situation becomes more complicated.

The global data set collected for different lithospheric plates and different oceans by Stein and Stein [1992] shows that, for ages less than 75 Ma, the age–depth curves for the South America plate, the part of the Pacific plate north of the Equator, and the Northwest Atlantic plate are very similar. Plates older than 75 Ma demonstrate irregular behavior: their depths differ considerably from the average age–depth curve. This is apparently caused by other tectonic processes, the most important among them probably being mantle plumes, which cause additional heating and uplift of the oceanic lithosphere. Another possible explanation for the different behavior of older plates is that the thermal parameters of basalt, which is believed to be the main building material of the oceanic lithosphere, change considerably from place to place and also exhibit a strong dependence on pressure and temperature (for detailed data, see [Touloukian et al., [1989]).

For forearc basins, it is sufficient to take into account the blanketing effect of sediments, which can exceed 15 km in thickness. A model of a cooling half-space takes into account the effect of sedimentation, as well as the release of latent heat at the lithosphere–asthenosphere boundary and corresponding subsidence resulting from crystallization of the basalt melt [Mikhailov and Timoshkina, 1993]. A statement of the problem, its analytical solution, and parameters for lithosphere of different ages are presented in the Appendix. The solution provides an age–depth curve that falls within the range of values tabulated in the global data set of Stein and Stein [1992].

We applied this model to the wells and measured section shown in Fig. 2 to estimate subsidence from an assumed initial distribution of temperature in the forearc lithosphere at the beginning of subduction. The age of the ophiolites exposed in the Coastal Ranges is about 150 Ma [Hopson et al., 1981]; thus, subsidence is the result of cooling of the forearc lithosphere during the last 75 Ma and is equal to the increase in depth of a typical ocean as its age increases from 75 to 150 Ma. According to the map of the basement depths of [Wentworth et al., 1995], the thickness of sediments exceeds 14 km for the area of the Peter Cook #13 well and the Mt. Diablo outcrop (curves *2* and *4*, respectively). This yields 0.68 km of water-filled thermal subsidence for the last 75 Ma, or 0.47 km of unloaded (no water fill) subsidence. For the area of wells 1 and 3, the thickness of sediments is considerably less. It reduces the thermal blanketing effect and yields 0.78 km of water-filled

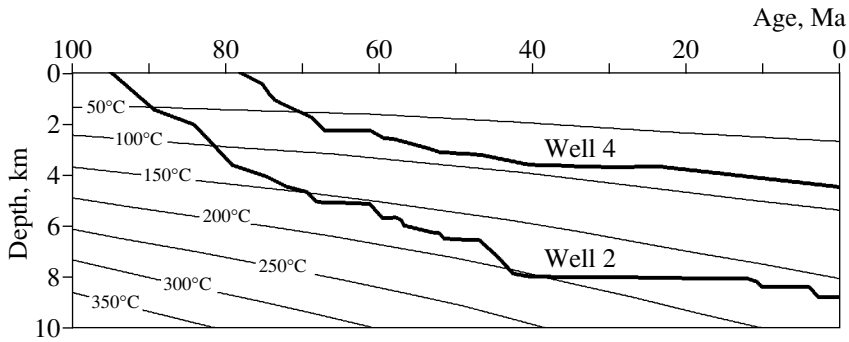

Fig. 6. Curves of total subsidence (uncorrected for subsidence under the weight of sedimentary layers) for well 2 and outcrop section 4, plotted on the background of a diagram demonstrating changes in temperature with depth and time (thin lines) according to the thermal model of a forearc lithosphere. The sedimentary rocks in the Upper Cretaceous–Tertiary layers of the Sacramento Delta area (age < 100 Ma) have never been hotter than 200°C, which was predicted by Zieglar and Spotts [1978] using results of organic matter analysis.

thermal subsidence, or 0.55 km of unloaded subsidence. It is worth noting that, in the absence of sediments, there is 0.83 km of water-filled thermal subsidence, so that neglecting sedimentation increases subsidence of the forearc basin by up to 0.15 km. Such increases are significant for our modeling.

4.4. Comparison to Subsidence of the Sacramento Valley

Comparing results of our thermal modeling, we find that the total thermal subsidence of a forearc basin formed on an oceanic lithosphere (equal to the sum of subsidence resulting from forearc dynamics and from cooling of the oceanic lithosphere) corresponds well to the long-term component of subsidence for the Mt. Diablo outcrop (4) and well 2 (Fig. 2). According to our estimates, separation of the thermal problem into two parts leads to negligible errors. The subsidence shown in well 3, situated east of outcrop 4, and in well 1 to the northeast at the northern border of the Sacramento Valley appears to be considerably less and can be approximated by the subsidence resulting from the dynamics of the subduction zone alone. A possible explanation is that the lithosphere of the Sacramento Delta area differs from the lithosphere of other parts of the valley, being closer to normal oceanic lithosphere of age 150 Ma. We will return to this question in the discussion after comparing results of our thermal modeling with data on the present-day and paleo heat flow and temperatures.

5. DISCUSSION

5.1. Comparison with Heat Flow and Paleotemperature Observations

If the Sacramento Delta lithosphere is oceanic lithosphere of age 150 Ma, our thermal model predicts the following:

(i) Present-day heat flow should be 30 mW/m^2, which agrees with heat flow measurements in this area (see Section 2.3). This predicted heat flow value is obtained for areas of a high sedimentation rate (as in well 2 and outcrop 4); for a slower sedimentation rate (as in wells 1 and 3), the present-day heat flow would be 32 mW/m^2. In our calculations we did not take into account possible heat generated radioactively within the Franciscan turbidites; this contribution might increase heat flow by up to 7 mW/m^2.

(ii) The thermal gradient should have changed from 32°C/km at 70 Ma to 18.4°C/km at present. This is in good agreement with values suggested by Zieglar and Spotts [1978], who estimated the thermal gradient during the Upper Cretaceous–Tertiary to be in the range 22–36°C/km. These gradients also fall within the range of the present-day average thermal gradient for the Sacramento Valley, estimated by Lico and Kharaka [1983] to be 18–25°C/km.

Figure 6 shows the changes in temperature gradient over time predicted by the thermal model for the Sacramento Delta area and the total subsidence curves for wells 2 and outcrop 4 (without correction for subsidence under the weight of sedimentary layers). According to this plot, sedimentary rocks in the Upper Cretaceous–Tertiary layers of the Sacramento Delta area have never been hotter than 200°C. This agrees with the conclusion of Zieglar and Spotts [1978] based on organic matter analysis in the Tertiary and Cretaceous sediments (see Section 2.3 for more details). Good agreement of the thermal model with observed subsidence rates and data on paleo and present-day heat flow and thermal gradients suggests that our model can be used to estimate the strength of the lithosphere at various depths.

5.2. Strength of the Crust in the Sacramento Delta Region; Comparison to Seismicity

Strength diagrams were calculated assuming diabase rheology for the Sacramento Delta crust and olivine rheology for the upper mantle. We used a conven-

tional approach (e.g., [Ranalli, 1997]), estimating the strength of the lithosphere at different depths as the minimum differential stress $\sigma = \sigma_1 - \sigma_3$ calculated either by Coulomb failure theory for frictional behavior of rocks with preexisting fractures (Byerlee's law),

$$\sigma = \alpha\rho g z(1-\lambda), \quad (1)$$

or by the Dorn equation for exponential temperature dependence of creep,

$$\sigma = (\dot{\varepsilon}/A_D)^{1/n}\exp\left(\frac{E}{nRT}\right), \quad (2)$$

where α is a fault type factor; ρ is the average density of overlying rocks; g is the gravity acceleration; z is depth; and λ is a pore fluid factor, defined as the ratio of pore fluid pressure to lithostatic (overburden) pressure. In the Dorn equation, $\dot{\varepsilon}$ is the strain rate; A_D, n, and E are empirically determined parameters, assumed not to vary with stress; pressure, or temperature; $R = 8.317$ J/(K mol) is the universal gas constant; and T is the temperature (K). The values assumed for these parameters in our calculations are described in the next paragraphs.

If we assume that the relative plate velocity changes from 4 cm/yr in the vicinity of the San Andreas fault to zero in the Great Valley region over a distance of approximately 100 km, then over that interval the strain rate is approximately 1.3×10^{-14} s^{-1}, which is in reasonable agreement with other estimates for the San Andreas region. For example, using the amplitude of displacements during earthquakes, the shear stress accumulation rate on the San Andreas fault has been estimated to be $\dot{\varepsilon} = 10^{-14}$ s^{-1}, while using regional geodetic data for the whole region, the strain rate was estimated as 3×10^{-14} s^{-1} (for discussion and references, see [Turcotte and Schubert, 1982]). Unruh and Lettis [1998] used focal mechanism data from the Coast Ranges to estimate a rate of compression in the direction perpendicular to the Hayward fault of 2–3 mm/yr and a rate of movement along this fault of 6–8 mm/yr. The width of the region where these deformations occur is about 40 km, yielding a strain rate of $\dot{\varepsilon} = 5 \times 10^{-15}$ s^{-1}. Taking into account these uncertainties, we calculated strength diagrams for strain rates ranging from 10^{-14} to 10^{-16} s^{-1}.

Based on focal mechanisms reported by Wong [1987], we used a transcurrent fault type factor (α = 1.2). The pore fluid pressure was assumed to be hydrostatic; i.e., the factor λ was set equal to 0.4. It is difficult to estimate the strength of the sedimentary section because of a dearth of experimental data on power creep for these types of rocks. To make matters worse, there are many indicators of high pore fluid pressures in the Great Valley sedimentary layers (for references, see Beyer [1988]). Thus, for the sedimentary section, the upper 15 km of the strength diagrams shown in Fig. 7 should be considered as an upper limit.

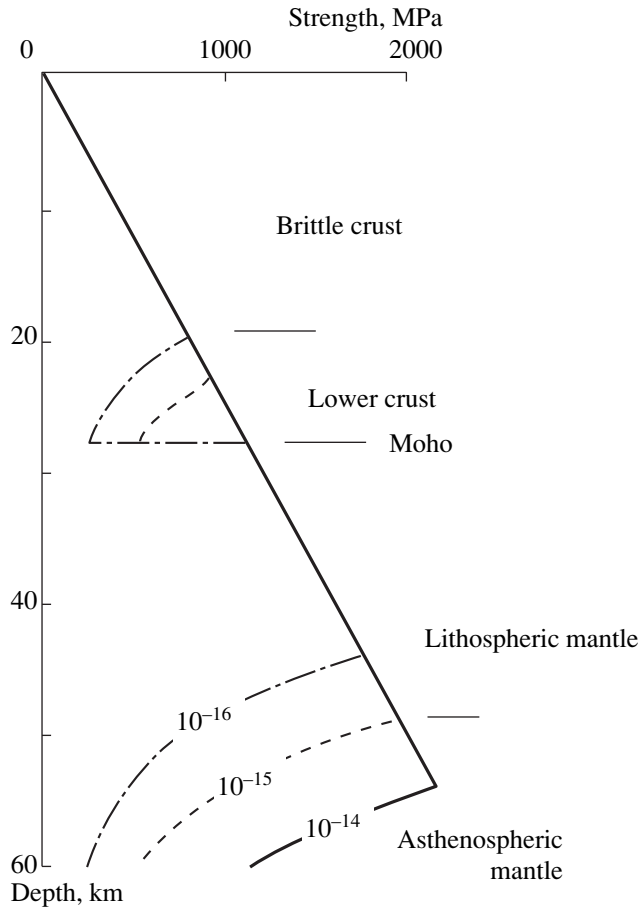

Fig. 7. Strength diagrams for the Sacramento Delta region assuming diabase rheology for the crust and wet olivine rheology for the lithospheric mantle. See text for parameters and discussion. Note that over a wide range of strain rates strength diagrams predict brittle layers at the base of the crust and below the Moho. (Note that Byerlee's law (1) probably overestimates rock strength at the pressure typical for the mantle.)

For the mantle rheology, we used creep parameters appropriate to wet olivine. Wet olivine rheology is not commonly used for describing mantle rheology because, being heated, rocks lose water very rapidly. However, wet olivine rheology may be appropriate to the present study area because for a long time it was situated above a shallow subducting oceanic plate. In this geodynamic environment, we assume upward movement of volatile components to the base of the Great Valley lithosphere. For wet olivine rheology, we used the following values [Evans and Kohlstedt, 1995]: $A_D = 10^{-3.3}$ MPa^{-n} s^{-1}, $n = 3.0$, and $E = 420$ kJ/mol. For dry diabase rheology we used $A_D = 10^{-3.7}$ MPa^{-n} s^{-1}, $n = 3.4$, and $E = 260$ kJ/mol [Kirby and Kronenberg, 1987a, 1987b]. Resulting strength diagrams for the upper 60 km of the Great Valley lithosphere are shown in Fig. 7. The upper part of the diagrams was constructed using diabase rheology. The distribution of

temperature corresponds to the Sacramento Delta lithosphere.

For the high strain rate (10^{-14} s^{-1}), all the crust is rigid, so there could be a strong, seismogenic layer from the top of the Sacramento Delta crystalline basement down to the Moho discontinuity and below into the mantle. As the strain rate decreases, a ductile layer appears in the lower part of the crust: for a strain rate of 10^{-15} s^{-1} the brittle–ductile transition occurs at a depth of 22 km, and for 10^{-16} s^{-1}, at a depth of 20 km. As a result, we can conclude that even slow deformation in the upper part of the Sacramento Delta crust can cause brittle failure, which is in agreement with seismological data. The rheology of the mantle below the Moho also appears to be brittle; even Byerlee's law (1) probably overestimates rock strength at the pressure typical for the mantle.

6. CONCLUSIONS

Seismic profiles and well data suggest that the Sacramento Delta lithosphere differs from the lithosphere under other parts of the Great Valley. Results of subsidence modeling of a forearc basin developed on oceanic lithosphere of age 150 Ma show good agreement with the observed subsidence history of the Sacramento Delta region. This model also predicts past and present-day temperatures and heat flow that are in good agreement with existing data. Thus, we conclude that the lithosphere under the Sacramento Delta may resemble normal oceanic lithosphere, whereas the lithosphere of the eastern and northern parts of the Great Valley, by virtue of its thickness and subsidence history, could be considered as some transitional rather than oceanic type. This transitional lithosphere was probably created as a result of Middle–Late Jurassic obduction of oceanic lithosphere onto the lithosphere of the Sierrian volcanic belt (e.g., [Godfrey et al., 1997]).

Differences in the structure and thermal history of the lithosphere under the Sacramento Delta region offer a possible explanation for the unusually deep (~20 km) seismic events in this area. According to strength estimates from our thermal modeling, the Sacramento Delta lithosphere contains a strong seismogenic layer at the base of the crust and below the Moho even for very slow strain (deformation) rates. Thus the upper part of the crystalline crust in this region (at least down to 20–22 km) can fail in brittle fashion, in agreement with seismological data. The greater width of the seismogenic zone in this area raises the possibility that earthquakes of somewhat greater magnitude might occur on fault segments of comparable length when compared to the Coast Ranges to the west. Magnitude–area relations suggest that an increase in seismogenic thickness of 50% would lead to an increase in magnitude of almost 0.2 units for a fixed segment length.

APPENDIX

Thermal Model of Oceanic Lithosphere

Suppose that the oceanic lithosphere consists of three layers (Fig. A1):

(1) a sedimentary layer having density ρ_0 (at T = 0°C), thermal conductivity λ_0, and thermal diffusivity a_0 and with an upper surface that coincides with the ocean floor;

(2) a crystalline lithosphere with density, thermal diffusivity, and thermal conductivity equal to ρ_1, λ_1, and a_1, respectively, with its top coinciding with the surface of the oceanic crust;

(3) an asthenospheric layer with parameters ρ_2, λ_2, and a_2, and with a top that we will assume to be a phase boundary at which basalt melt crystallizes.

We use a non-Cartesian system of coordinates with the Ox axis running along the top of the oceanic lithosphere, the vertical axis Oz pointing downward, and the origin of the coordinates being in the spreading center at the top of the oceanic basement. If t, the age of the oceanic lithosphere, is known (by magnetic anomalies, for example), we can replace the distance from the spreading center by the age of the oceanic lithosphere. We denote the relief of the sedimentary layer as $\varsigma_s(t) \leq 0$ and that on the top of the asthenosphere as $\varsigma_a(t) \geq 0$. Moving from the center of the rift zone, the lithosphere subsides under the weight of the thickening sedimentary layer and also as a result of increasing thickness of the cooling lithosphere if the density of the lithosphere is larger than that of the asthenosphere ($\rho_1 > \rho_2$). It is easy to demonstrate that for oceanic lithosphere one can neglect the decrease in the thermally driven subsidence with depth (the total thermal subsidence is included in the model by assuming that the axis Ox runs along the top of the lithosphere). We can also neglect horizontal heat transfer in the oceanic lithosphere and sedimentary layer [Turcotte and Schubert, 1982].

Under these assumptions, the thermal evolution of oceanic lithosphere can be described by the following system of equations:

$$a_i \frac{\partial^2 T_i}{\partial z^2} = \frac{\partial T}{\partial t}, \quad i = 0, 1, 2, \tag{A.1}$$

where in the sedimentary layer $i = 0$, $\varsigma_s(t) < z \leq 0$; in the lithosphere $i = 1$, $0 < z \leq \varsigma_a(t)$; and in the asthenosphere $i = 2$, $z > \varsigma_a(t)$. Thus $T_0(z, t)$ is the temperature in the sedimentary layer and $T_1(z, t)$ and $T_2(z, t)$ are the temperatures of the crystalline lithosphere and asthenosphere, respectively.

Initial and boundary conditions are as follows:

(1) at the spreading center (t = 0): $T_2(z, 0) = T_a$, where T_a is the temperature of the asthenosphere (we will use T_a = 1350°C);

(2) at the oceanic floor: $T_0(\varsigma_0(t), t)$ = 0°C;

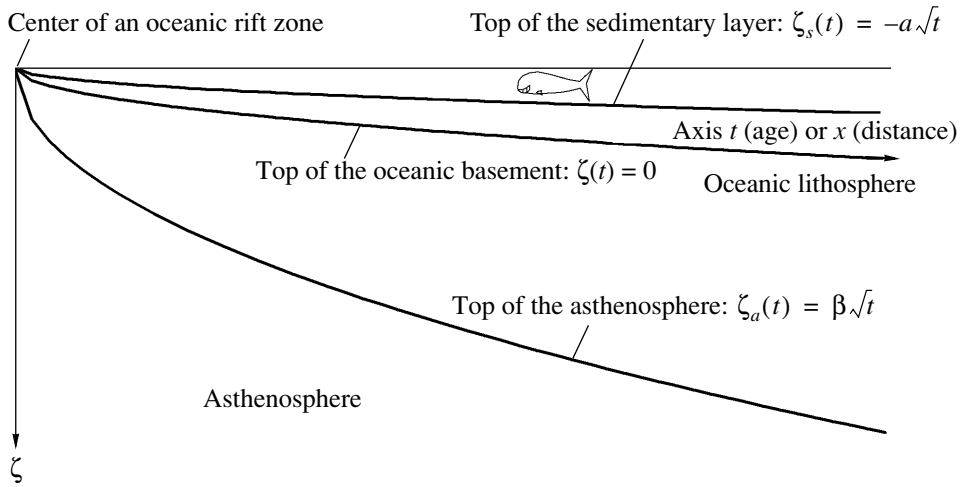

Fig. A1. Thermal model of an oceanic rift zone.

(3) continuity of temperature at the surface of the basement $T_0(0, t) = T_1(0, t)$ and at the base of the lithosphere $T_1(\varsigma_a(t), t) = T_2(\varsigma_a(t), t) = T_f$, where T_f is the solidus temperature of basalt;

(4) continuity of heat flow at the oceanic basement $(z = 0)$, $\lambda_0 \frac{\partial T_0}{\partial z} = \lambda_1 \frac{\partial T_1}{\partial z}$;

(5) the Stefan condition at the base of the lithosphere, when $\varsigma = \varsigma_a(t)$:

$$\mu L \rho_2 \frac{\partial \varsigma_a(t)}{\partial t} = \left(\lambda_1 \frac{\partial T_1}{\partial z} - \lambda_2 \frac{\partial T_2}{\partial z}\right), \quad \text{(A.2)}$$

where L is the specific heat of basalt crystallization and μ is the concentration of liquid basaltic phase, expressed as a fraction.

The solidus temperature of oceanic basalts collected at different sites varies from 1060°C to 1250°C. It also depends on pressure and the character of this dependence is determined by the presence of volatiles [Touloukian et al., 1989]. The liquidus temperature of basalt also depends on the pressure, but the difference between solidus and liquidus temperatures depend only weakly on pressure; thus, for a first-order approximation, we can consider the difference $T_a - T_f$ to be a constant. To arrive at an analytical solution, let us assume that the thickness of the sedimentary layer may be expressed as a function of the square root of the age, i.e., $\varsigma_s(t) = -\alpha\sqrt{t}$. (This function should describe the main temporal trend of the sedimentary wedge growth; short-term variations are not important.) In this case, the depth to the phase boundary is also proportional to the square root of the age, $\varsigma_a(t) = \beta\sqrt{t}$, and the thermal problem has a simple analytical solution [Batsanin and Golmshtok, 1986]:

$$T_i(z, t) = A_i + B_i \mathrm{erf}(z/2\sqrt{a_i t}), \quad i = 0, 1, 2, \quad \text{(A.3)}$$

where erf(…) is the probability integral.

From the boundary and initial conditions we derive

$$A_0 = A_1 = T_f e_0/(e_0 + \gamma e_1),$$
$$B_0 = A_0/e_0 = B_1/\gamma, \quad A_2 = (T_f - T_a e_2)/(1 - e_2),$$
$$B_2 = T_a - A_2,$$

where $\gamma = \frac{\lambda_0}{\lambda_1}\sqrt{\frac{a_1}{a_0}}$, $e_0 = \mathrm{erf}\left(\frac{\alpha}{2\sqrt{a_0}}\right)$, $e_i = \mathrm{erf}\left(\frac{\beta}{2\sqrt{a_i}}\right)$, $i = 1, 2$.

From the Stefan condition we obtain an equation to determine β when the thermal parameters ($a_1, \lambda_1, a_2, \lambda_2, L, \mu$) of the model layers and the sedimentation parameter (α) are known:

$$\frac{\lambda_1}{\sqrt{a_1}} B_1 \exp(-\beta^2/4a_1) - \frac{\lambda_2}{\sqrt{a_2}} B_2 \exp(-\beta^2/4a_2) = \frac{\sqrt{\pi}}{2}\mu L \rho_2 \beta. \quad \text{(A.4)}$$

Integrating the temperature along the vertical axis from the top of the sedimentary layer to infinity, one obtains the thermal subsidence $H_T(t)$:

$$H_T(t) = \sqrt{t} k_T \frac{2}{\sqrt{\pi}}[B_2\sqrt{a_2} e^{-\beta^2/4a_2} - B_1\sqrt{a_1}(e^{-\beta^2/4a_1} - 1)]. \quad \text{(A.5)}$$

The total subsidence as a result of crystallization of the basalt melt and increase in lithospheric thickness can be obtained from the condition of local isostatic equilibrium as

$$H_{\mathrm{is}}(t) = (H_T(t)\rho_2 + H_{\mathrm{cr}}(t)(\rho_4 - \rho_3)\mu/2 + \beta\sqrt{t}(\rho_1 - \rho_2))/(\rho_2 - \rho_w), \quad \text{(A.6)}$$

where $H_{is}(t)$ is the water-filled depth to the top of the oceanic basement relative to the initial depth in the spreading center ($t = 0$) corrected for subsidence under sedimentary weight. $H_{cr}(t)$ is subsidence as a result of crystallization of the basalt melt; ρ_w is the water density, ρ_3 is the basalt melt density, ρ_4 is the density of basalt, and k_T is the thermal expansion coefficient. The density of the basalt melt depends on the pressure [Touloukian et al., 1989] and grows almost linearly, approaching the density of solid basalt at about 60 km depth. (To account for this growth, the coefficient of $H_{cr}(t)$ in Eq. (A.6) was divided by two.) The term containing $H_{cr}(t)$ is important when modeling subsidence of young oceanic lithosphere. We used this term when calibrating our model against the global data set and dismissed it when estimating subsidence of the forearc lithosphere from 75 to 150 Ma.

We conclude that, under the assumptions listed above, the depth to the oceanic basement, the thickness of the lithosphere, and thermal and isostatic (water-filled) subsidence are proportional to the square root of the age of the oceanic lithosphere (with coefficients dependent on time because both pressure and temperature are time-dependent) plus a term containing $H_{cr}(t)$, which grows rapidly up to ~40 Ma, after which it becomes constant. The temperature of the mantle does not change considerably in this model, so the thermal parameters of the mantle can be treated as constants. In the absence of volatiles, the liquidus temperature of basalt grows with pressure [Touloukian et al., 1989]. Subsidence of the lithosphere is slightly dependent on the liquidus temperature of basalt, but this parameter increases the average temperature of the lithosphere and as a result decreases its thermal conductivity and diffusivity (they both decrease with increasing temperature). To account for these temporal dependences, we used the following model parameters:

$$L = 0.419 \times 10^6 \text{ J/kg};\ k_T = 3 \times 10^{-5}\ ^\circ\text{C}^{-1};\ \mu = 5\%;$$

$$\rho_0 = 2.4 \text{ Mg/m}^3,\ \rho_1 = \rho_2 = 3.3 \text{ Mg/m}^3;\ \rho_4 = 2.9 \text{ Mg/m}^3;$$

$$\lambda_0 = 1.75 \text{ W/(m °C)},\ \lambda_2 = 2.5 \text{ W/(m °C)};$$

$$a_0 = 5 \times 10^{-7} \text{ m}^2\text{/s},\ a_2 = 7 \times 10^{-7} \text{ m}^2\text{/s; and}$$

$$\text{when } t < 50 \text{ Ma},\ \lambda_1 = 2.5 \text{ W/(m °C)};$$

$$a_1 = 5.5 \times 10^{-7} \text{ m}^2\text{/s};\ T_f = 1060^\circ;\ \rho_3 = 2.6 \text{ Mg/m}^3;$$

$$\text{when } t \geq 50 \text{ Ma},\ \lambda_1 = 2.1 \text{ W/(m °C)};$$

$$a_1 = 4.8 \times 10^{-7} \text{ m}^2\text{/s};\ T_f = 1250^\circ;\ \rho_3 = 2.9 \text{ Mg/m}^3.$$

Numerical calculations demonstrate the low sensitivity of age–depth curves to assumed values of thermal conductivity and to solidus and liquidus temperatures of basalt. The rate of subsidence depends mainly on the thermal diffusivity of the lithosphere and mantle and also on the amount and density of the basalt melt for young oceanic lithosphere. The resulting age–depth curve falls within the uncertainty limits given by a global database for oceanic lithosphere ages up to 150 Ma [Stein and Stein, 1992].

ACKNOWLEDGMENTS

We thank L. Beyer, E.E. Brabb, T.M. Brocher, S.A. Graham, S. Kirby, W.D. Mooney, N. Sleep, and C.M. Wentworth for sharing their data and knowledge on the Great Valley. The work of V. Mikhailov on this project was supported by the USGS Russian–American Cooperative program.

REFERENCES

1. W. H. Bakun, "Seismic Activity of the San Francisco Bay Region." Bull. Seismol. Soc. Am. **89**, 764–784 (1999).
2. S. F. Batsanin and A. Ya. Golmshtok, "On Thermal Evolution of Oceanic Lithosphere with Sedimentation," Okeanology **XXIV** (4), 654–658 (1986).
3. H. M. Benz, G. Zandt, and D. H. Oppenheimer, "Lithospheric Structure of Northern California from Teleseismic Images of the Upper Mantle," J. Geophys. Res. **97**, 4791–4807 (1992).
4. L. A. Beyer, *Summary of Geology and Petroleum Plays Used to Assess Undiscovered Recoverable Petroleum Resources of Sacramento Basin Province, California* (USGS Spec. Rep. 88-4500-oo, 1988).
5. L. A. Beyer and J. A. Bartow, *Summary of Geological and Petroleum Plays Used to Assess Undiscovered Recoverable Petroleum Resources, San Joaquin Basin Province, California* (USGS Open File Rep. 87-450-Z, 1987).
6. R. G. Bohannon and T. Parsons, "Tectonic Implications of Post-30 Ma Pacific and North American Relative Plate Motion," Geology **107**, 937–959 (1995).
7. E. E. Brabb, C. L. Powell II, and T. M. Brocher, *Preliminary Compilation of Data for Selected Oil Wells in Northern California* (USGS Open File Rep. 01–152, 2001).
8. S. J. H. Buiter, R. Govers, and M. J. R. Wortel, "A Modelling Study of Vertical Displacements at Convergent Plate Margins," Geophys. J. Int. **147**, 415–427 (2001).
9. P. J. Coney and S. J. Reynolds, "Cordilleran Benioff Zones," Nature **279**, 403–406 (1977).
10. J. H. Davis, "Simple Analytic Model for Subduction Zone Thermal Structure," Geophys. J. Int. **139**, 823–828 (1999).
11. E. E. Davis and C. R. B. Lister, "Fundamentals of Ridge Crest Topography," Earth Planet. Sci. Lett. **21**, 401–413 (1974).
12. J. P. Devaux, L. Fleitout, G. Schubert, and Ch. Anderson, "Stress in a Subducting Slab in the Presence of a Metastable Olivine Wedge," J. Geophys. Res. **105**, 13 365–13 373 (2000).
13. W. R. Dickinson and W. S. Snyder, "Geometry of Subducted Slabs Related to San Andreas Transform," J. Geol. **87**, 609–627 (1979).
14. W. R. Dickinson, R. A. Armin, N. Beckvar, et al., "Cenozoic Basin Development of Coastal California," in *Cenozoic Development of Coastal California: Rubey Vol. VI*,

Ed. by R.V. Ingersol and W.G. Ernst (Prentice-Hall, New Jersey, 1987), pp. 1–23.

15. T. A. Dumitru, "Constraints on Uplift in the Franciscan Subduction Complex from Apatite Fission Track Analysis," Tectonics **8**, 197–220 (1989).
16. T. Dumitru, "Effects of Subduction Parameters on Geothermal Gradients in Forearcs, with Application to Franciscan Subduction in California," J. Geophys. Res. **96**, 621–641 (1991).
17. J. P. Eaton, "Crustal Structure from California to Eureka, Nevada, from Seismic-Refraction Measurements," J. Geophys. Res. **68**, 5789–5806 (1963).
18. W. L. Ellsworth, G. C. Beroza, B. R. Julian, et al., "Seismicity of the San Andreas Fault System in Central California: Application of the Double-Difference Location Algorithm on a Regional Scale," Eos Trans. AGU **81**, 919 (2000).
19. D. C. Engebretson, A. Cox, and R. G. Gordon, "Relative Motions between Oceanic and Continental Plates in the Pacific Basin," Geol. Soc. Am. Spec. Paper **206**, 148–165 (1985).
20. B. Evans and V. Kohlstedt, "Rheology of Rocks," in *Rock Physics and Phase Relations. A Handbook of Physical Constants, AGU Reference Shelf 3*, Ed. by T. J. Ahrens (1995), pp. 148–165.
21. K. Furlong, "Lithospheric Behavior with Triple Junction Migration: An Example Based on the Mendocino Triple Junction," Phys. Earth Planet. Int. **36**, 213–223 (1984).
22. N. J. Godfrey, B. C. Beaudoin, S. L. Klemperer, and Mendocino Working Group, "Ophiolitic Basement to the Great Valley Forearc Basin, California, from Seismic and Gravity Data: Implications for Crustal Growth at the North America Continental Margin," Geology **108**, 1536–1562 (1997).
23. S. A. Graham, "Tectonic Controls on Petroleum and Hydrocarbon Occurrence, Sacramento Valley, California," in *Cenozoic Development of Coastal California: Rubey Volume VI*, Ed. by W. G. Ernst (1987), pp. 47–63.
24. B. U. Haq, J. Hardenbol, and P. R. Vail, "Chronology of Fluctuating Sea Levels since the Triassic (250 Ma Ago to Present)," Science **235**, 1156–1167 (1987).
25. R. N. Hey, H. W. Menard, T. M. Atwater, and D. W. Caress, "Changes in Direction of Seafloor Spreading Revisited," J. Geophys. Res. **93**, 2803–2811 (1988).
26. W. S. Holbrook and W. D. Mooney, "The Crustal Structure of the Axis of the Great Valley, California, from Seismic Refraction Measurements," Tectonophysics **140**, 49–63 (1987).
27. W. S. Holbrook, T. M. Brocher, U. S. Brink, and J. A. Hole, "Crustal Structure of a Transform Plate Boundary: Bay and the Central California Continental Margin," J. Geophys. Res. **101**, 22311–22334 (1996).
28. J. A. Hole, T. M. Brocher, S. L. Klemperer, et al., "Three-Dimensional Seismic Velocity Structure of the Bay Area," J. Geophys. Res. **105**, 13857–13874 (2000).
29. S. Honda, "Thermal Structure beneath Tohoku, Northeast Japan—A Case Study for Understanding the Detailed Thermal Structure of the Subduction Zone," Tectonophysics **112**, 69–102 (1985).
30. C. A. Hopson, J. M. Mattison, and Jr. E. A. Pessagno, *Coast Range Ophiolite, Western California: Englewood Cliffs* (USGS Open File Rep. 88-45-O, 1981).
31. A. Hsui and N. Toksoz, "The Evolution of the Thermal Structures beneath a Subduction Zone," Tectonophysics **60**, 43–60 (1979).
32. R. V. Ingersol, "Evolution of the Late Cretaceous Forearc Basin Northern and Central California," Geol. Soc. Am. Bull. **90**, 813–826 (1979).
33. R. C. Jachens, A. Griscom, and C. W. Roberts, "Regional Extent of the Great Valley Basement West of the Great Valley. California: Implications for Extensive Tectonic Wedging in the California Coastal Ranges," J. Geophys. Res. **100**, 12769–12790 (1995).
34. S. H. Kirby and A. K. Kronenberg, "Rheology of the Lithosphere: Selected Topics," Rev. Geophys. Space Phys. **25**, 1219–1244 (1987a).
35. S. H. Kirby and A. K. Kronenberg, "Correction to Rheology of the Lithosphere: Selected Topics," Rev. Geophys. Space Phys. **25**, 1680–1681 (1987b).
36. A. H. Lachenbruch and J. H. Sass, "Heat Flow and Energetics of the San Andreas Fault Zone," J. Geophys. Res. **85**, 6185–6223 (1980).
37. M. G. Langseth, J. X. Le Pichon, and M. Ewing, "Crustal Structure of the Mid-Ocean Ridges. 5. Heat Flow through the Atlantic Ocean Flow and Convection Currents," J. Geophys. Res. **71**, 5321–5355 (1966).
38. M. S. Lico and Y. K. Kharaka, "Subsurface Pressure and Temperature Distribution in Sacramento Basin, California," in *Selected Papers of the Pacific Section 1983 Annual Meeting, Sacramento, California*, Ed. by R. Hester and D. E. Hellinger (Pacific section, AAPG, 1, 1983) pp. 57–75.
39. J. McCarthy, P. E. Hart, R. Anima, et al., "Seismic Evidence for Faulting in the Western Sacramento Delta Region, Pittsburg, California," Eos Trans. AGU **75** (1994).
40. D. P. McKenzie, "Some Remarks on Heat Flow and Gravity Anomalies," J. Geophys. Res. **72**, 6261–6273 (1967).
41. D. P. McKenzie, "Speculations on the Consequences and Causes of Plate Motions," Geophys. J. R. Astron. Soc. **8**, 1–32 (1969).
42. D. P. McKenzie, "Temperature and Potential Temperature beneath Island Arcs," Tectonophysics **10**, 357–366 (1970).
43. V. O. Mikhailov and E. P. Timoshkina, "Analysis of Data on the Nansen Cordillera, Assuming a Thermal Model of an Oceanic Lithosphere," Proc. (Doklady) Russ. Acad. Sci. **331**, 497–499 (1993).
44. W. D. Mooney and C. S. Weaver, "Regional Crustal Structure and Tectonics of the Pacific Coastal States; California, Oregon, and Washington," in *Geophysical Framework of the Continental United States*, Ed. by L. A. Pakiser, and W. D. Mooney (Geol. Soc. Am. Mem., 172, Washington, DC, 1989), 129–162.
45. I. W. Moxon, Stratigraphic and Structural Architecture of the San-Joaquin, Sacramento Basins, *PhD Thesis*, Stanford University, California, 1990.
46. I. W. Moxon and S. A. Graham, "History and Controls of Subsidence in the Late Cretaceous-Tertiary Great Valley Forearc Basin, California," Geology **15**, 626–629 (1987).
47. D. R. H. O'Connell, J. R. Unruh, and L. V. Block, "Source Characterization and Ground-Motion Model-

ling of the 1892 Vacaville-Winters Earthquake Sequence, California," Bull. Seismol. Soc. Am. **91**, 1471–1497 (2001).

48. D. H. Oppenheimer and N. Macgregor-Scott, "The Seismotectonics of the Eastern San Francisco Bay Region," in *Proc. 2nd Conf. on Earthquake Hazards in the Eastern San Francisco Bay Area,* Ed. by Borchardt, Glenn, and others (California Department of Conservation, Division of Mines and Geology Special Publication, Vol. 113, 1992), pp. 11–16.
49. B. M. Page and D. C. Engebretson, "Correlation between the Geological Record and Computed Motion for Central California," Tectonics **3**, 133–155 (1984).
50. B. M. Page and T. M. Brocher, "Thrusting in the Central California Margin vver the Edge of the Pacific Plate during the Transform Regime," Geology **21**, 635–638 (1993).
51. R. L. Parker and D. W. Oldenburg, "Thermal Model of Ocean Ridges," Nat. Phys. Sci. **242**, 137–139 (1973).
52. T. Parsons, A. M. Trehu, J. H. Luetgert, et al., "A New View into the Cascadia Subduction Zone and Volcanic Arc: Implications for Earthquake Hazards along the Margin," Geology **26**, 199–202 (1998).
53. S. Peacock, "Thermal and Petrologic Structure of Subduction Zones," in *Subduction from Top to Bottom,* Ed. by G. E. Bebout, D. W. Schroll, S. H. Kirby, J. P. Platt (AGU Geophys. Monogr. Vol. 96, 1996), pp. 119–133.
54. C. Prodehl, *Crustal Structure of the Western United States* (USGS Prof. Pap. 1034, 1979).
55. R. N. Pysklywec and M. C. L. Quintas, "A Mantle Flow Mechanism for the Late Paleozoic Subsidence of the Parana Basin," J. Geophys. Res. **105**, 16359–16370 (2000).
56. G. Ranalli, "Rheology of the Lithosphere in Space and Time," in *Orogeny through Time (Geol. Soc. Spec. Public. 121),* Ed. by J.-P. Burg and M. Ford (1997), pp. 19–37.
57. J. H. Sass, A. H. Lachenbruch, R. J. Munroe, et al., "Heat Flow in the Western United States," J. Geophys. Res. **76**, 6378–6413 (1971).
58. J. H. Sass, S. P. Galanis, Jr., and R. J. Munroe, *easurement of Heat Flow by a Downhole Probe Technique in the San Joaquin Valley, California* (USGS Open-File Rep. 76–56, 1982).
59. J. H. Sass, C. F. Williams, A. H. Lachenbruch, et al., "Thermal Regime of the San Andreas Fault Near Parkfield, California," J. Geophys. Res. **102**, 27575–27585 (1997).
60. D. W. Scholl, R. von Huene, T. L. Vallier, and D. G. Howell, "Sedimentary Masses and Concepts about Tectonic Processes at Underthrust Oceanic Margins," Geology **8**, 564–568 (1980).
61. J. Severinghaus and T. Atwater, "Cenozoic Geometry and Thermal State of the Subducting Slabs beneath Western North America. Basin and Range Extension," Geol. Soc. Am. Mem. **176**, 1–22 (1990).
62. J. E. Spencer, "A Numerical Assessment of Slab Strength during High- and Low-Angle Subduction and Implications for Laramide Orogeny," J. Geophys. Res. **99**, 9227–9236 (1994).
63. B. Stam, F. M. Gradstein, P. Lloyd, and D. Gillis, "Algorithms for Porosity and Subsidence History," Comput. Geosci. **13**, 317–349 (1987).
64. C. Stein and S. Stein, "A Model for the Global Variation in Oceanic Depth and Heat Flow with Lithospheric Age," Nature **359**, 123–129 (1992).
65. J. M. Stock and P. Molnar, "Uncertainties and Implications of the Late Cretaceous and Tertiary Position of North America Relative to the Farallon, Kula, and Pacific Plates," Tectonics **7**, 1339–1384 (1988).
66. Y. S. Tuloukian, W. R. Judd, and R. F. Roy, *Physical Properties of Rocks and Minerals, CINDAS Data Series on Material Properties, II-2* (1989).
67. D. L. Turcotte and G. Schubert, *Geodynamics: Application of Continuum Physics to Geological Problems* (Wiley, 1982).
68. M. B. Underwood, "Temporal Changes in Geothermal Gradient, Franciscan Subduction Complex, Northern California," J. Geophys. Res. **94**, 3111–3125 (1989).
69. J. R. Unruh and W. R. Lettis, "Kinematics of Transpressional Deformation in the Eastern Bay Region, California," Geology **26**, 19–22 (1998).
70. J. van der Beukel and R. Wortel, "Thermo-Mechanical Modelling of Arc–Trench Regions," Tectonophysics **154**, 177–193 (1988).
71. J. Wang and R. J. Munroe, *Heat Flow and Sub-Surface Temperatures in the Great Valley, California* (USGS Open-File Rep. 82–844, 1982).
72. J. Weber-Band, P. L. Williams, D. L. Jones, et al., *Active Tectonic Deformation at the Eastern Margin of the California Coast Ranges: Results of the BASIX and CALCRUST Programs* (USGS Open-File Rep. 97–691, 1997).
73. C. M. Wentworth, M. D. Zoback, A. Griscom, et al., "A Transect across the Mesozoic Accretionary Margin of the Central California," Geophys. J. Int. **85**, 105–110 (1987).
74. C. M. Wentworth and M. D. Zoback, "The Style of the Late Cenozoic Deformation at the Eastern Front of the California Coastal Ranges," Tectonics **8**, 237–246 (1989).
75. C. M. Wentworth, G. R. Fisher, P. Levine, and R. C. Jachens, *The Surface of the Crystalline Basement, Great Valley, Sierra Nevada, California: A Digital Map Database* (USGS Open File Rep. 95-96, 1995).
76. C. F. Williams and S. P. Galanis, Jr., *Heat-Flow Measurements in the Vicinity of the Hayward Fault, California* (USGS Open-File Rep. 94–692, 1994).
77. T. Williams, Basin-Fill Architecture and Forearc Tectonics, Cretaceous Great Valley Group, Sacramento Basin, Northern California, *Ph.D. Thesis*, Stanford University. California, 1997.
78. I. G.Wong, "Earthquake Activity in the Sacramento Valley, California and Its Implications To Active Geological Structures and Contemporary Tectonic Stress," in *Structural Geology of Sacramento Basin (Annual Meeting of Pacific Section, Am. Assoc. Pet. Geol., Sacramento, California, 1987),* Ed. by V. B. Cherven and W. F. Edmondson, pp. 5–14.
79. I. G. Wong, R. W. Ely, and A. C. Kollman, "Contemporary Seismicity and Tectonics of the Northern and Central Coast Ranges–Sierran Block Boundary Zone, California," J. Geophys. Res. **93**, 7813–7833 (1988).
80. D. L. Zieglar and J. H. Spotts, "Reservoir and Source-Bed History of Great Valley, California," Am. Assoc. Pet. Geol. Bull. **62**, 813–826 (1978).